ISSN 8755-6839

SCIENCE OF **TSUNAMI HAZARDS**

Journal of Tsunami Society International

Volume 33 **Number 2** **2014**

VALIDATION OF THE JRC TSUNAMI PROPAGATION AND INUNDATION CODES

N. Zamora
GeoForschungsZentrum (GFZ), Germany

G. Franchello and A. Anunziato
EC-Joint Research Centre (JRC), Italy

ABSTRACT

In the last years several numerical codes have been developed to analyse tsunami waves. Most of these codes use a finite difference numerical approach giving good results for tsunami wave propagation, but with limitations in modelling inundation processes. The HyFlux2 model has been developed to simulate inundation scenario due to dam break, flash flood and tsunami-wave run-up. The model solves the conservative form of the two-dimensional shallow water equations using a finite volume method. The implementation of a shoreline-tracking method provides reliable results. HyFlux2 robustness has been tested using several tsunami events. The main aim of this study is code validation by means of comparing different code results with available measurements. Another objective of the study is to evaluate how the different fault models could generate different results that should be considered for coastal planning. Several simulations have been performed to compare HyFlux2 code with SWAN-JRC code and the TUNAMI-N2. HyFlux2 has been validated taking advantage of the extensive seismic, geodetic measurements and post-tsunami field surveys performed after the Nias March 28th tsunami. Although more detailed shallow bathymetry is needed to assess the inundation, diverse results in the wave heights have been revealed when comparing the different fault mechanism. Many challenges still exist for tsunami researchers especially when concern to early warning systems as shown in this Nias March 28th tsunami.

Keywords: *fault scenarios, tsunami propagation, HyFlux2 code.*

Vol. 33, No. 2, page 112 (2014)

1. INTRODUCTION

Tsunami wave propagation has been an important focus of study since the significant studies of Mader (1974). In the last two decades many numerical code have come to light using different numerical approaches. Developers have improved robustness by testing different numerical methods. Moreover, seismological data and tsunami surveys have helped to validate the reliability of these codes with the important application coastal planning and tsunami early warning.

A mega-thrust earthquake magnitude 8.6 occurred on March 28th, 2005 with epicentre at Nias Island at 16:10:31 UTC (around 110 km to the SE of the 12/26/2004 earthquake). The earthquake triggered a tsunami with maximum 3 m run-up at Simeulue Island, a 2 m run-up at Nias Islands and 1 m Singkil and Meulaboh in Sumatra Main Island. Red tsunami alert was sent by the European Commission Global Disaster Alert and Coordination System (GDACS) 16 minutes after the event. The Joint Research Centre of the European Commission (JRC) has developed different types of tsunami calculations such as the near-real time calculations, the grid scenarios calculations and the post event calculations. When a new event is detected by the seismological sources (e.g. USGS, EMSC), an evaluation is performed to estimate the importance of the event from humanitarian point of view. This is important for the needs of alert systems. Fault models, their selection and the best automatic process for alerting systems have been a great challenge. Slip distribution is one of the main inputs for a reliable tsunami numerical simulation this research intends to evaluate different fault models and also numerical code performance. Besides, improvement of alerting systems has driven to consider the applications of Global Positioning Systems (GPS) into tsunami early warning systems since they can measure ground motions in real time every few seconds (Sobolev et al., 2007; Song, 2007; Falck et al., 2010). The measurements from GPS in buoys could allow an almost real-time detection of tsunami waves offshore. This offshore data attached with onshore GPS that determines ground movements are of great importance and started to be implemented (Falck, 2010). Implementation of such new methods joined with actual fault mechanism analysis could address to acquire more reliable deformation data in near real-time-earthquake occurrence. However, up to now this information is not integrated in GDACS retrieving systems or databases that consider seismological data available.

Therefore, near field tsunami events are an important source to assess the accuracy of ground deformation models which provides the input of the hydrodynamic models. Given that an important amount of scientific data is available from post-event field surveys, geodetic measurements and seismological data, we have the aim to make an evaluation of the tsunami propagation and inundation numerical codes used at the JRC.

We present comparisons of several post-event calculations done with three different numerical codes. In addition, fault scenario tsunami inundation differences along the coast are evaluated. Simulations have been performed to compare the results obtained by the SWAN-JRC code (Annunziato, 2005; 2007), the TUNAMI-N2 (Imamura, 2006) and the HyFlux2 (Franchello, 2008). The event was simulated by defining the initial conditions by means of the Finite fault model (Ji et al, 2002) and the fault solution of Okada Fault Model using the Global Harvard Moment Tensor solution (gCMT).The Northern Sumatra earthquake (Nias event) is a good example to understand and to evaluate the

performance and reliability of these numerical codes in earthquakes occurring very close to the coast and in which tsunami alert is a challenge due to the small time available to alert communities.

As has been known from historic data and recent events, this region is a prone area for generation of earthquakes and tsunamis. Sunda region is a typical island-arc structure with a deep oceanic trench, a volcanic inner arc and a marginal basin. This region is one of the most seismically active regions in the world owing to the confluence of multiple plates moving at high relative speeds (McCaffrey, 2009).The rate of subduction varies along the trench being 5.9 cm/yr in South Sumatra and 5.3 cm/yr along the Indo-Australian plate subducting beneath Burma and Sunda plate (Prawirodirdjo and Bock, 2004; Subarya et al., 2006). In the last 35 years, 12 earthquakes with magnitudes greater to M*w* 7.4 have occurred along western Indonesia (Fig. 1.1).

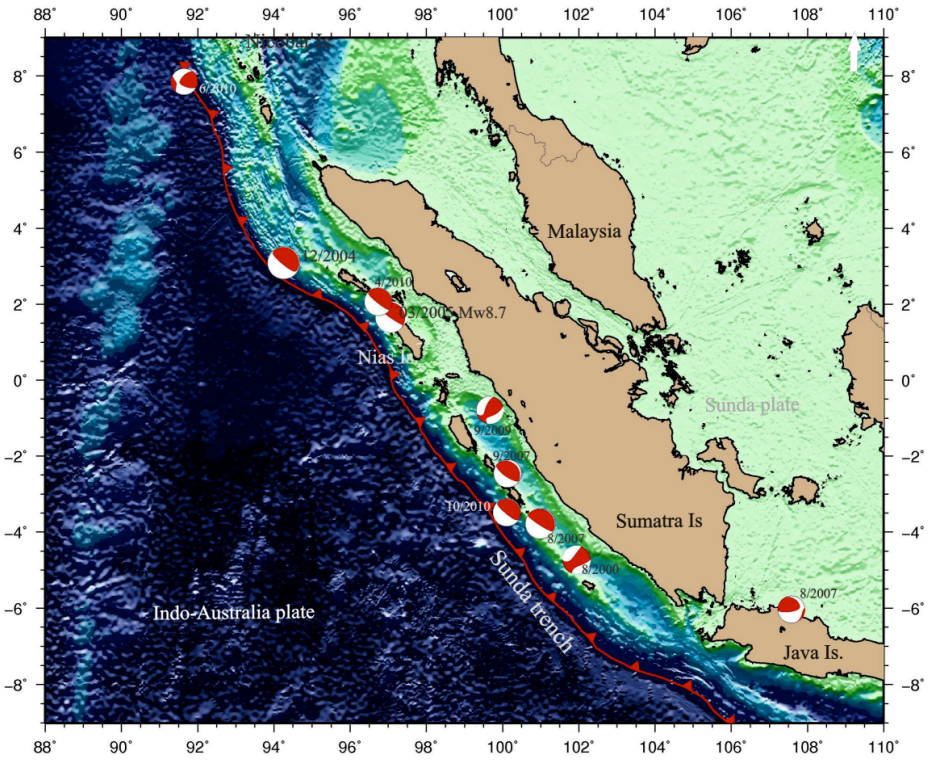

Figure 1.1. Sunda trench and gCMT earthquakes Mw>7.4 from 01/1976 - 01/2012.

2. CODES AND METHODS

Numerical approaches when apply to tsunami modeling have advantages and disadvantages concerning their applications to wave propagation, inundation or risk management. For further discussion about differences of numerical codes refers to Castro et al. (2012). Herein, we consider three numerical codes available at EC-JRC. The numerical codes SWAN-JRC, TUNAMI-N2 and HyFlux2 solve the shallow water equations using different numerical methods: SWAN and TUNAMI use the finite different method (FDM) while HyFlux2 uses the finite volume (FVM).

The shallow water equations are commonly used to describe tsunami wave propagation and general features of the inundation processes. These equations can be derived using different approximations, all of which relies on the assumption that the flow is vertically hydrostatic, the vertical velocity and the vertical acceleration are negligible. The fluid is incompressible, the water temperature is constant and the pressure at the free surface is constant.

The *SWAN-JRC code* (Annunziato, 2007) solves the shallow water equations by the finite difference numerical scheme based on SWAN Mader code (1988). This code has been implemented for *Global Disaster Alerts and Coordination System (*GDACS). The SWAN-JRC code estimates the fault length, height and direction to determine the initial water displacement. The code initializes the calculation space, performs the travel time propagation calculation, verify at each step if there are locations reached by the wave and thus update the visualization and animation files. For early warning purposes of GDACS the model can run in automatic mode and publish automatically the results in the GDACS web site. For post event calculations the Global Centroid Moment Tensor solutions (gCMT) and Finite Fault Model (FFM) as well as other earthquake parameters can be used to compare or improve simulation results.

The *TUNAMI-N2 code* was developed by the Disaster Control Research Center through the Tsunami Inundation Exchange Modeling (TIME) Program (Goto et al., 1997). It is based on the shallow water equations solved by a finite difference numerical scheme. The TUNAMI code consists of several codes. However in this project we have used the TUNAMI-N2 (linear theory in deep sea, non-linear shallow-water theory in shallow sea and run-up on land with constant grids). In this analysis TUNAMI-N2 has been used. TUNAMI-N2 code is included in the JRC Tsunami suite and therefore the results can be easily produced with the same environment as the SWAN code (Annunziato, 2005).

The HyFlux2 model has been developed to simulate severe inundation scenario due to dam break, flash flood and tsunami-wave run-up. The model solves the conservative form of the two-dimensional shallow water equations using a finite volume method. The interface flux is computed by a Flux Vector Splitting method for shallow water equations based on a Godunov-type approach. A second-order scheme is applied to the water surface level and velocity. Physical models are included to deal with bottom steps and shorelines. The second-order scheme together with the shoreline-tracking method makes the model well balanced in respect to mass and momentum conservation laws, providing reliable and robust results (Franchello, 2010). In relation to ground deformation mass conservation both the bathymetry change and sea level change must be applied. In HyFlux2 it is assumed an instantaneous and equal deformation applied for bathymetry and water level.

The coastal flooding and inundation are commonly simulated by extending propagation calculations perform with a nested grid approach. The code requires as input detailed information on seismic source mechanisms, gridded bathymetric data for the open sea propagation, and a set of gridded Digital Elevation Models (DEM) containing detailed bathymetry and topography in order to model the inundation phase. The most common procedure to track movements of the shoreline (Imamura, 1996; Liu et al., 1998; Imamura et al., 2006) is the moving boundary treatment. Run-up is calculated with nonlinear computations. The numerical codes such as TUNAMI-N2, among others, use the

moving boundary approach in inundation quantification. In contrast, HyFlux2 uses a shoreline tracking method to model the interface between dry and wet. The inundation 2D scheme of HyFlux2 has been designed to identify the shoreline as intersection between two planar surfaces which describe the bottom and the water free surface (Franchello, 2010).

Using those available numerical codes we first, analyzed two rupture models (gCMT and FFM) compared with field data and geodetic measurements (e.g InSAR). In a second step, fault model is used to evaluate tsunami propagation by means of three numerical codes. At last, inundation is calculated using HyFlux2 code. Different bathymetry resolutions have been used. In order to reduce the calculation time, early warning system requires a rather coarse resolution (> 2.6 min). Resolutions of 0.5' are also used to evaluate propagation results. In one case 0.1' resolution has been used to compare wave heights with field measurements. HyFlux2 is included in the suite of codes that can be called upon by the JRC Tsunami suite, allowing an easy comparison of the code results (Zamora et al., 2011).

3. RESULTS AND DISCUSSION

3.1 Fault models

Fault parameters as initial condition in tsunami modeling are one of the major factors that determine the wave propagation and distribution of run-up along the coast. Therein the adopted approaches to estimate the initial conditions are based on algorithm that calculates analytical solution for surface deformation in an elastic half-space (Okada, 1985). This algorithm estimates the distribution of coseismic uplift and subsidence by using the hypocenter of the earthquake, strike, dip, rake and average displacement of the fault. The other approach is based on calculation of slip distribution by separating the fault plane into sub-faults (Ji et al., 2002).

In order to perform reliable tsunami simulations it is necessary to determine best fit fault models describing hypocenter, length and width of the fault, slip distribution and fault mechanism. The selection of the best fault model is especially hard in tsunami early warning context. This has driven to the need for evaluating fault mechanism for the March 28th, 2005 and to perform numerical codes performance comparisons using (1) the Harvard Global Centroid Moment Tensor (gCMT strike 329°, dip: 8°, rake: 109°), available few minutes to hours after the event and (2) the USGS Finite Fault Model (Ji et al., 2002) available few days after the event (Fig. 3.1).

InSAR deformation measurements for Nias earthquake show two main slip patches along Simeulue and Nias islands with maximum coseismic uplift of 2.5 m (Briggs et al., 2009). However, the FFM and gCMT parameters resulted in coseismic distribution overestimation in the case of FFM and subestimation of coseismic deformation when using gCMT parameters. Maximum vertical deformation calculated when using gCMT parameters is in agreement with InSAR 2.5 m (Fig. 3.1a). At the eastern part of Nias Island subsidence have been reproduced with the gCMT fault model, however with the InSAR measurements, uplift in the range of 0.5 m – 1.0 m is indicated exactly at Nias Island (Fig. 3.1). Comparably, subsidence is resulted for most of Nias Island when using FFM.

Vertical deformation is not consistent with InSAR measurement along Batu and Banyaks Islands, between Simeulue Island and Nias Island. At the eastern part of the Batu and Banyak Island subsidence has been estimated with FFM. However, this pattern is not consistent according to InSAR measurements (Fig. 3.1b). The static displacement field on the surface predicted by FFM is up to 3 m for uplift (Fig. 3.1b). Finally, the coseismic vertical deformation between the two fault scenarios differs in 1 m. If InSAR assessment is used as the base to compare deformation areas, main slip is very different for the two fault scenarios (gCMT and FFM). These results have important implication for tsunami early warning systems.

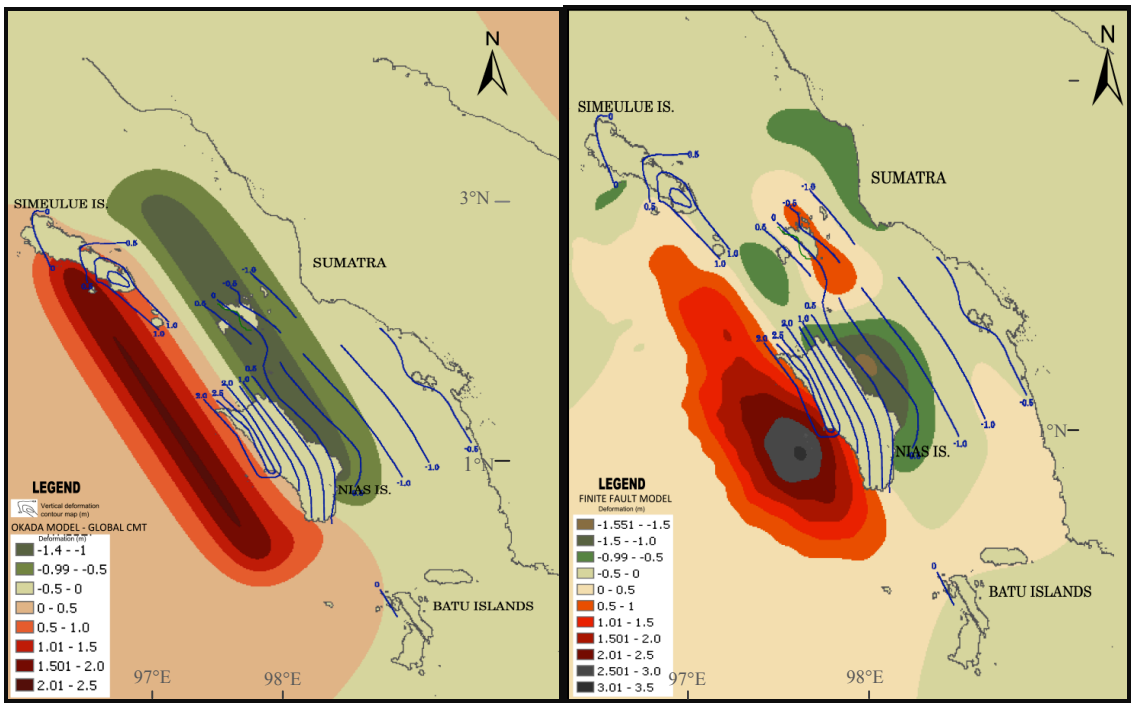

Figure 3.1. a. Resulted deformation using gCMT parameters in Okada Model. b. Fault deformation using FFM. The measured vertical deformation is shown by blue contours (from Briggs et al., 2009).

3.2 Calculation of wave using different fault models

It has been recognized that different hypocenter and slip distribution influence wave heights distribution along the coast. Therefore, simulations with gCMT model and FFM were performed to assess this difference wave heights resulted with SWAN-JRC simulations. Bathymetry grid of 900 m spatial resolution was used in these calculations.

The following map presents the location of the points where sea level is compared with the different fault models. At point S1 (behind Nias Island) amplitudes are very similar for both fault scenarios

(Fig. 3.2). At the S3 offshore point there is a small difference in time arrival of the first peak when comparing sea level trends resulted from the use of gCMT or Finite Fault Model. Because of location of point offshore the directivity and slip distribution is not affecting and therefore amplitudes are very similar on both fault models used in these simulations (Fig. 3.3).

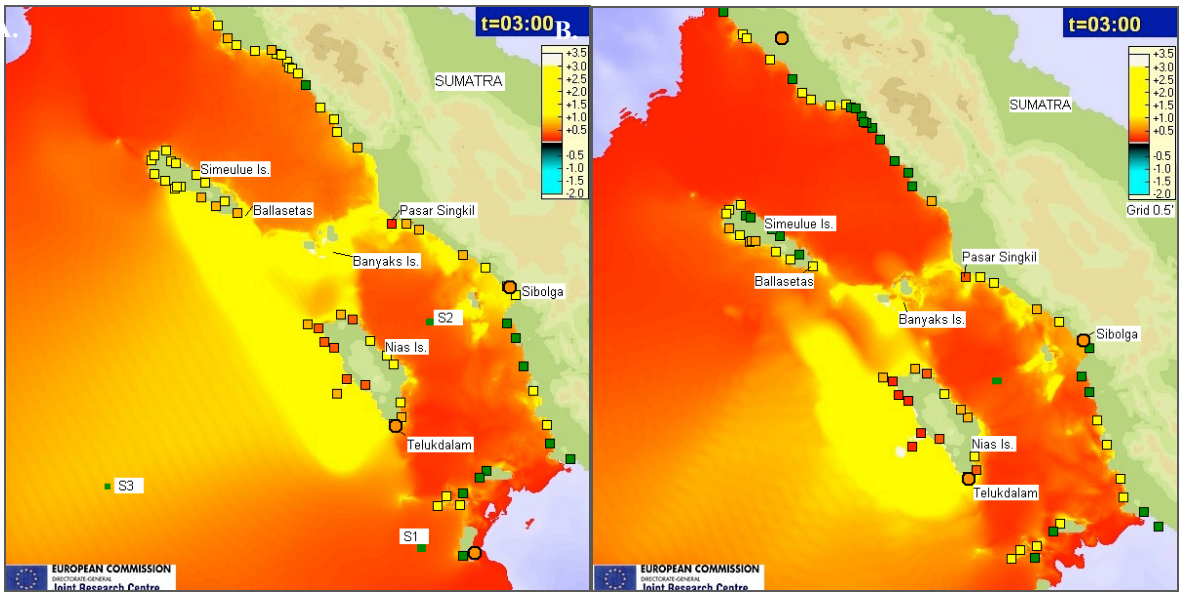

Figure 3.2. Maximum sea level resulted from simulations using two fault models a. Okada Model b. Finite Fault Model.

Arrival time of wave peak simulated using FFM is very similar when comparison is done at sites S1, S2 and S3 with offshore depths between -480 up to -4426 m (Fig. 3.4a). It is seen that most of the offshore directivity of wave is S-SW for FFM and SW for calculations performed using Okada model (Fig. 3.2).

Close to Ballesetas and Pasar Singkil the sea level trends differ for more than 1 m (Fig. 3.4b). This is related to the wave directivity caused by the fault orientation and by the slip patches (assessed by FFM). As expected, different focal mechanism and slip distribution resulted from Okada Model affect the initial wave profile. In addition, strike-directed slip variations could resulted in wave front-parallel changes in amplitude that are largely preserved during propagation from the source region toward shore causing refraction (Geist and Dmowska, 1999).

The following map shows a comparison of wave heights at selected coastal points (Fig. 3.. Wave height at these points were defined in a post processing step where the maximum wave height is acquired from a radius of 300 m to 1 km and for water depths close to 20 m. The main wave height differences at the shore are seen at Nias Island. This is related to slip coseismic distribution of each fault model.

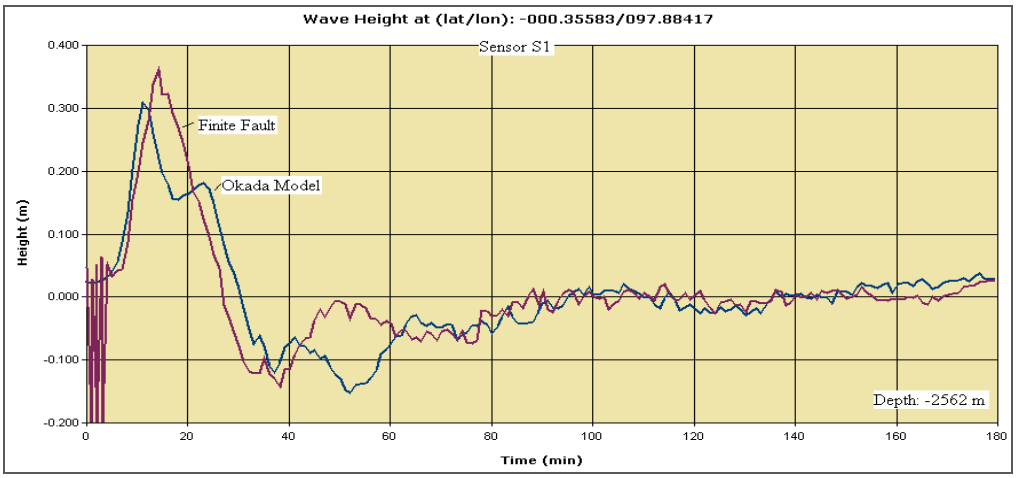

a. Comparison of wave heights offshore simulated with SWAN-JRC using two different fault models.

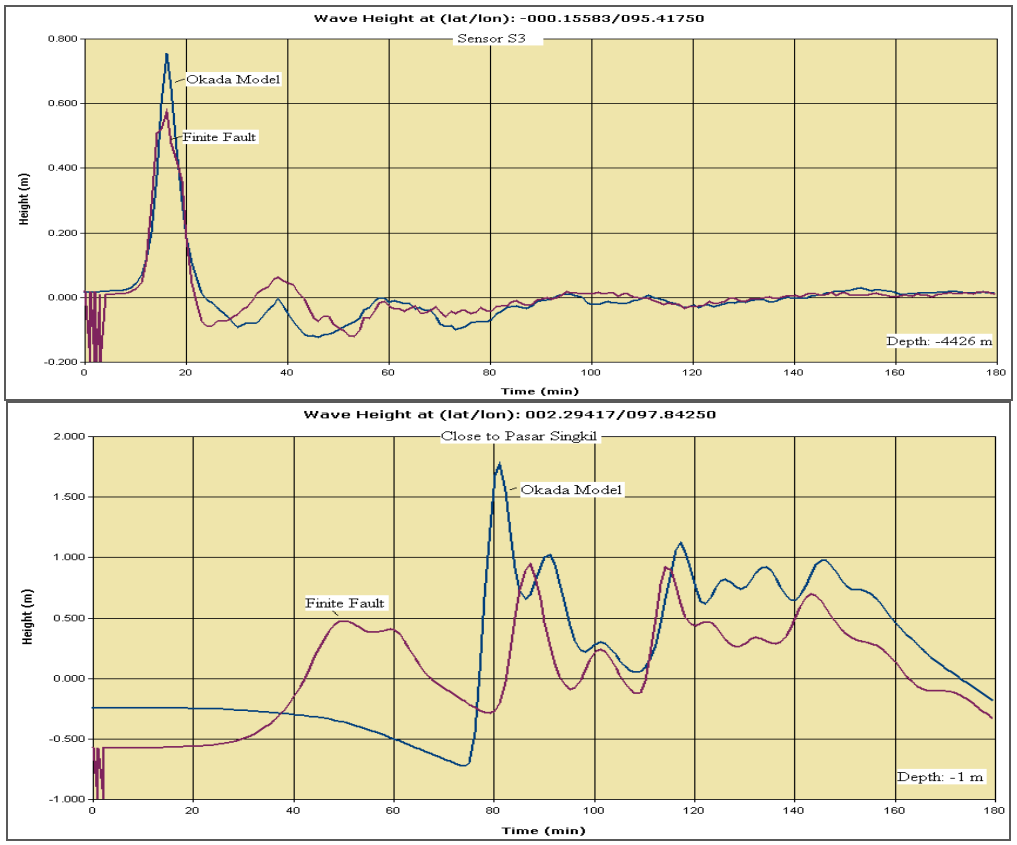

Figure 3.3.b. Comparison of wave heights close to shore. Simulations with SWAN-JRC using two different fault models.

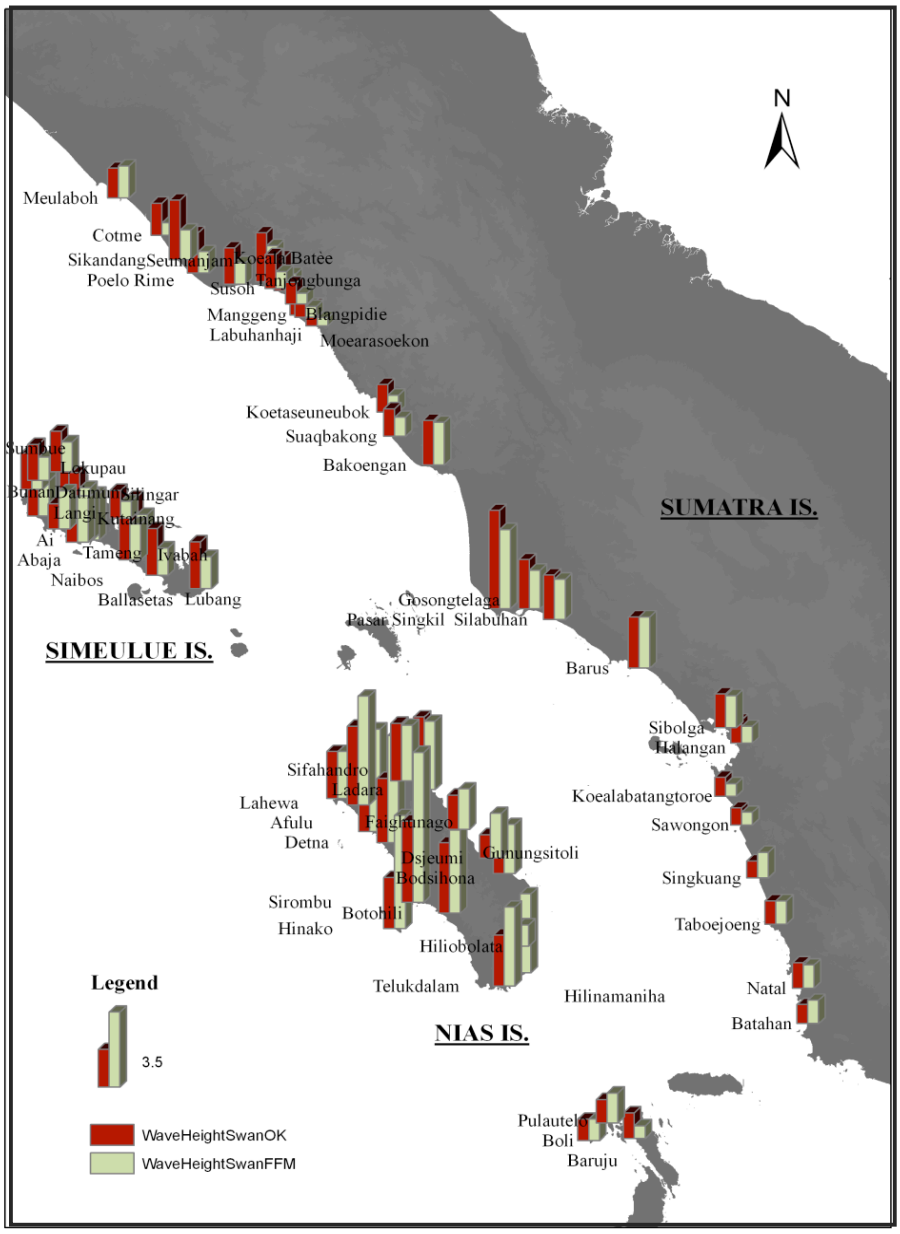

Figure 3.4. Maximum wave height resulted from 900 m bathymetry grid.

These differences in simulated wave height versus registered ones are related to the seafloor deformation characteristics (determination of fault mechanism), as observed especially for Nias Island where coseismic distribution from west to east varies from 1.5 m to -1.5 m on FFM and 1m uplift to -1.0 m east of Nias gCMT used on Okada Model.

3.3 Code to code assessment at 900 m resolution based on gCMT fault model

Sea level trends simulated at offshore (S2) point and at two sites close to shoreline are presented (Fig. 3.5). The objective is to compare wave height differences when using SWAN-JRC, HyFlux2 and TUNAMI-N2 numerical codes with gCMT parameters as input data. The calculation grid is 900 m. The maximum wave height recorded on simulation in point close to Telukdalam (Nias) arrives 11 minutes and 14 minutes after the earthquake according to SWAN-JRC and HyFlux2 respectively. At this point maximum wave height is 1.3 m (Fig. 3.5).

HyFlux2 code presents a smoother trend and differs for 3 minutes on first arrival compared to SWAN-JRC and TUNAMI-N2.

At location S2 the wave peak was recorded by SWAN-JRC code 18 minutes after the event. HyFlux2 code calculations registered the maximum height and first arrival at this point also 18 minutes after the event. Simulation with TUNAMI-N2 registered a wave 30 minutes after the event. Unfortunately no buoys were available to compare with real-time data.

As could be observed, HyFlux2 code results in shallow water do not show oscillations like the other codes. The smoother results can be due to the shoreline tracking method adopted in HyFlux2. In this sense, it is necessary to explain that HyFlux2 can provide 3 different values when performing simulations. These values are the maximum value of water height offshore (depth deeper than 20 m); the maximum value at shore (looking radius were determined from 300 m to 1 km along the shoreline) and the value inland. The more detailed bathymetric and topographic resolution, the smaller the radius on the coast needed for comparison and will drive to more reliable results for inundation assessment.

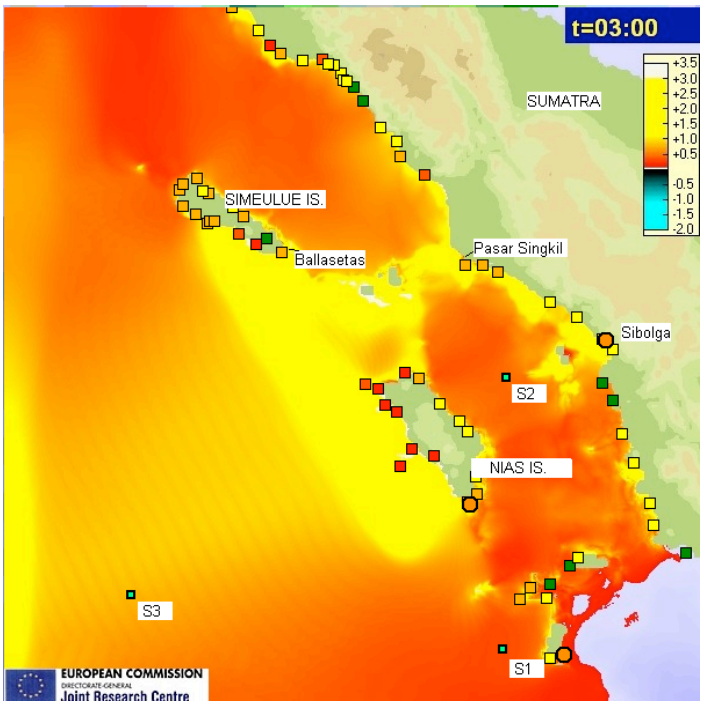

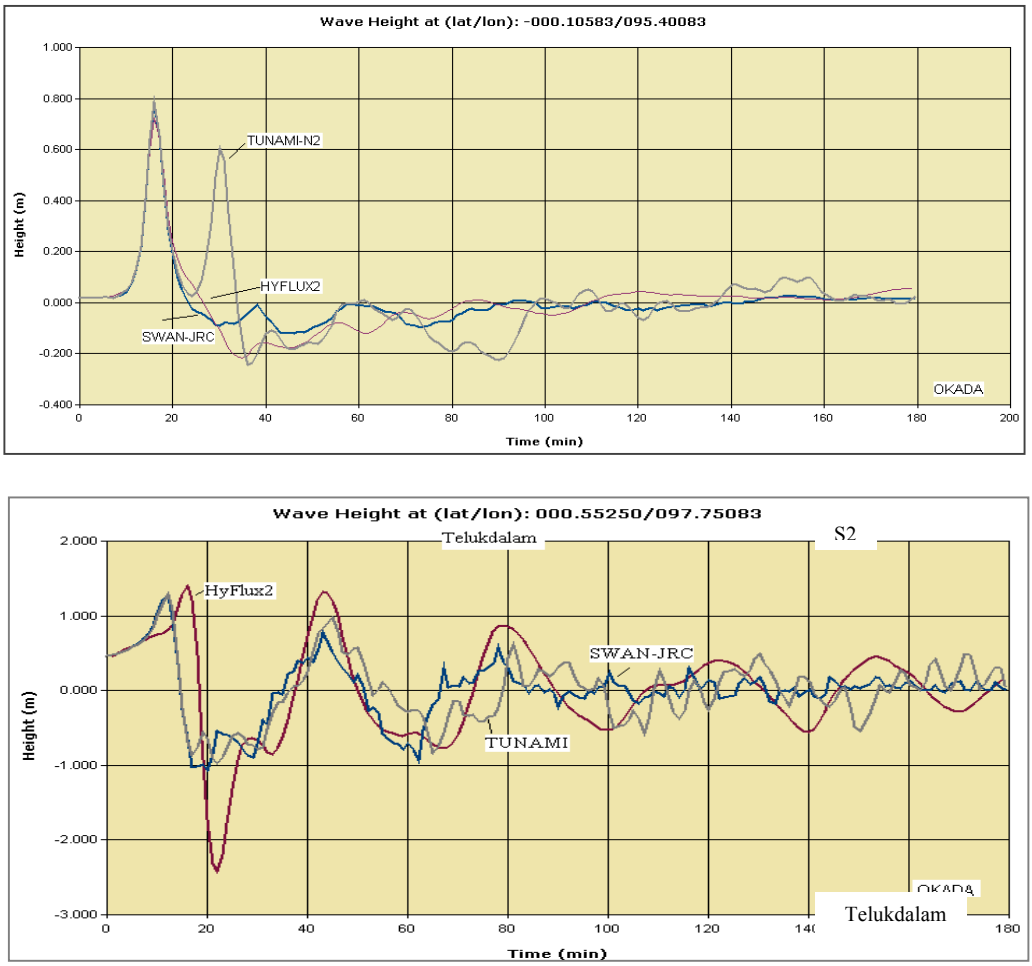

Figure 3.5. Maximum sea level resulted from HyFlux2 simulation using Okada Model.

From the sea level profiles shown above it has been concluded that the three numerical codes have similar behavior offshore. This does not apply when comparing HyFlux2 results with SWAN-JRC at very shallow waters sites, where the ratio (0.76)[1] of wave heights show wave heights with lower values HyFlux2 calculations. The ratio of HyFlux2 code calculations compared to TUNAMI-N2 is 0.6. Despite the fact that we tested that when wave heights simulated with HyFlux2 codes seem to be subestimated perhaps because we are using wave heights at shore. Moreover, when the so called zmaxShore (Fig. 3.6) provided by HyFlux2 post-processing is compared to the values given by SWAN-JRC, the ratio tend to be similar 1.11 (Fig. 3.8).

[1] The ratio has been calculated by AVERAGE[*wave height location values HyFlux2 code/ wave height location values SWAN-JRC*].

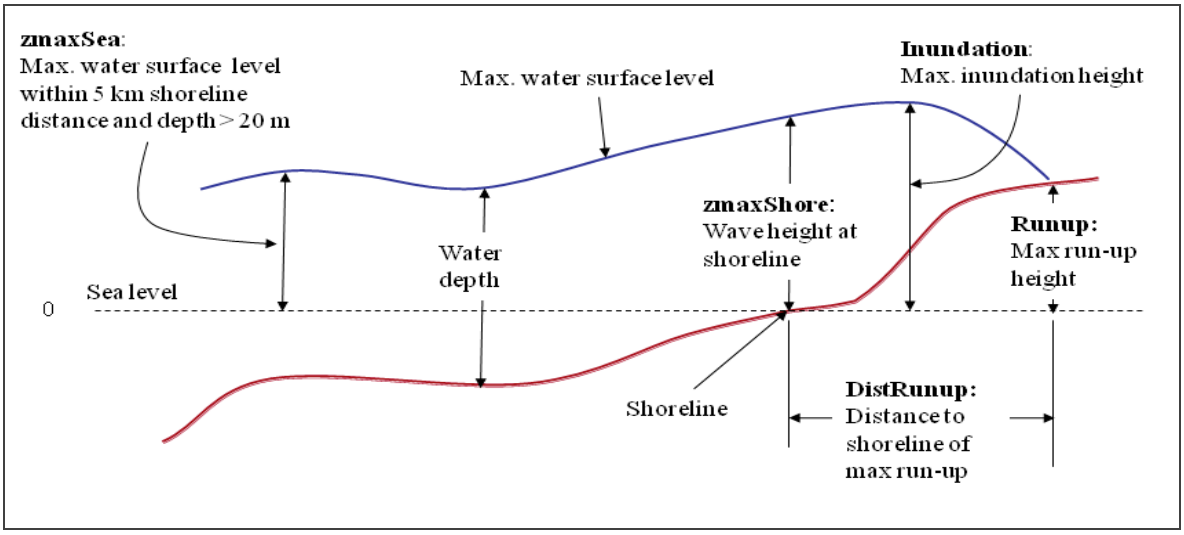

Figure 3.6. Sketch with definition of considred measurements (Franchello and Annunziato, 2012).

In the following maps wave height comparison of three codes is presented. This wave heights represented on the map are those resulted on heights higher than 0.5 m.

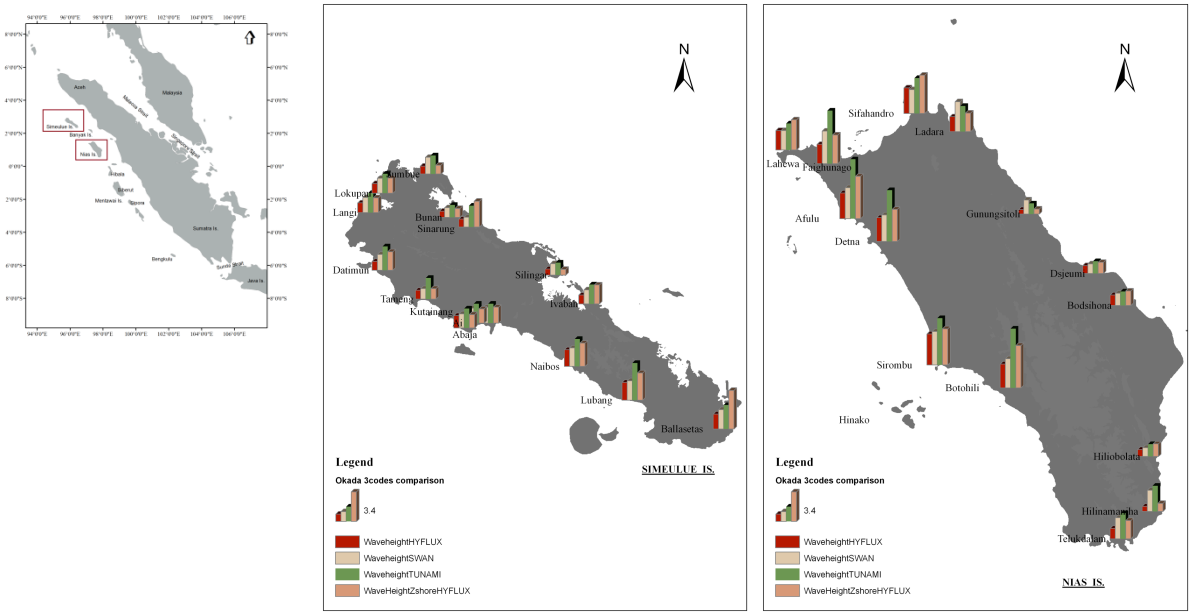

Figure 3.7. Comparison of simulated wave heights using different numerical codes using gCMT model. Grid size used in simulations is 900 m.

Wave height and inundation distance values are shown in figure 3.8. It could be seen that sites such as NW Nias are overstimated wave height zmaxShore is 3.42 m and measured wave height at this location is 0.5 m. Similarly at Banyaks, measurements are smaller than the simulated wave heights. On the contrary for Sibolga and along Sumatra coast wave height values are very similar (Fig. 3.8). These results confirm the importance to evaluate near field tsunamis, mainly for regions like western Indonesia with islands along main rupture area.

Finally, comparisons of the horizontal inundations measures with the simulations cannot be done because the maximum inundation extend is in the same order of magnitude of the grid size: the ratio between the horizontal inundation and the grid size should be at least 10, i.e. in order to capture an inundation of 300 m the grid size should be lower than 30 m (Franchello and Annunziato, 2012).

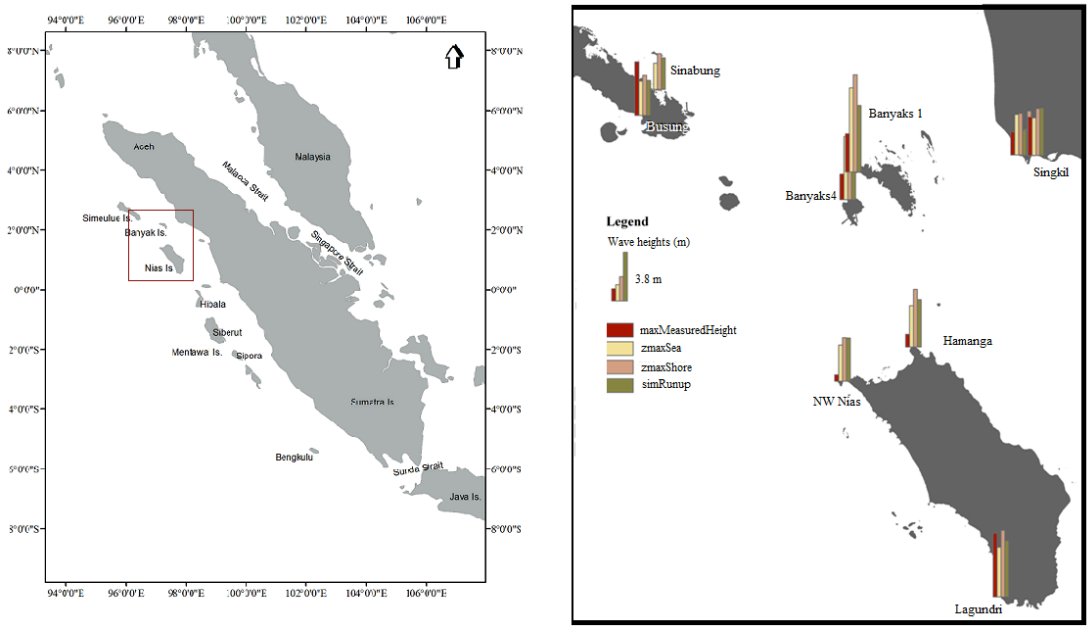

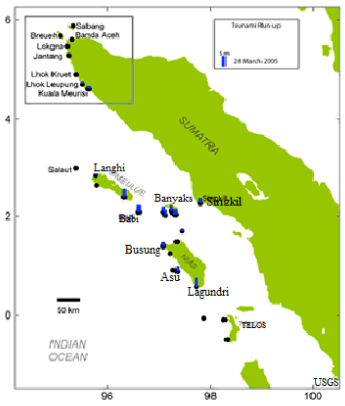

Site	Latitude	Longitude	maxMeasuredHeight	zmaxSea	zmaxShore	simulatedRunup
Sibolga	1.73	98.79	1.20	1.030	1.305	
Singkil	2.27	97.78	1.00	2.072	3.504	1.78
Langhi	2.82	95.74	0.50	1.630	1.723	
Busung	2.42	96.32	4.20	2.692	3.146	0.75
Babi	2.08	96.62	2.00	2.862	3.153	
Banyaks1	2.1	97.10	2.00	4.949	4.852	2.96
Banyaks4	2.05	97.10	2.00	3.854	4.519	
Singkil2	2.27	97.75	1.80	3.174	3.253	1.93
NW Nias	1.41	97.08	0.50	2.836	3.412	3.38
Lagundri	0.59	97.68	5.00	3.895	5.223	4.41
Asu	0.82	97.35	2.50	2.668	2.723	
Kariya Vhapi	2.83	95.74	3.20	1.557	1.709	
Sinabang	2.52	96.38	0.00	2.047	2.802	2.47
Port of Singkil	2.27	97.82	3.00	2.947	3.665	3.73
Hamanga beach	1.54	97.35	1.00	3.241	4.513	3.72
Lagundri Bay	0.57	97.75	4.00	2.363	3.042	

Figure 3.8. Selected points to show results of 900 m calculation. Simulated (sim) and measured (mes) values are shown. Water height and distances shown in meters.

3.4 Inundation assessment using HyFlux2

Within inundation assessment procedure many limitations are faced, mainly related to numerical scheme and bathymetry resolution. We have performed here simulations with available 300 m resolution. For more detailed bathymetry HyFlux2 code use resulting boundary conditions of previous coarser simulations.

Tsunami wave parameters close to the shoreline and inland can be measured with tidal gauges and with information acquired from field surveys after the event (USGS, 2005a). Tsunami evidence of the 2005 Nias tsunami was found along 500 km of the Indonesian coast. In this region the maximum run-up elevations were approximately 4 meters (USGS, 2005a).

We are aware that caution is needed when measured data is compared since the resolutions used for in this project are in the range of medium resolution. Thus one cannot expect to use this survey so punctual. However, it is important to use field data to have an idea of the bias of simulation results compared to what was measured on the field and using available bathymetry.

3.4.1 Singkil, Sumatra Island: grid 1

At Singkil-Baru site, NOAA-NGDC reported subsidence and 1 m water height. According to local reports, tsunami arrived 10 to 15 minutes after the earthquake and came as one large surge that stayed for almost an hour. Field watermark elevations were reported in the range of 1.5 to 1.8 m above the present sea level. The tsunami inundated approximately 200 m inland from the pre-earthquake shoreline (USGS, 2005a). Maximum simulated water height at Bankoengan is 2.15 m and 3.8 m at the Pasar Singkil. Simulation show good agreement with measured run-up (Fig. 3.9). The following chart (Table 1) shows the parameters used in the nested simulations.

Table 1. Parameters of simulation summarized.

Focal mechanism	Strike: 329°	Dip: 8°	Rake: 109 °	Slip: 6.4 m
Okada Model	Maximum coseismic uplift:			
Grid 1: 180 m resolution	Lon max: 98°	Lon min: 97°	Lat max: 3°	Lat min: 2°
Grid 2: 180 m resolution	Lon max: 96.5°	Lon min: 95.5°	Lat max: 3°	Lat min: 2°
Grid 3: 180 m resolution	Lon max: 98°	Lon min: 97°	Lat max: 1.5°	Lat min: 0.4°

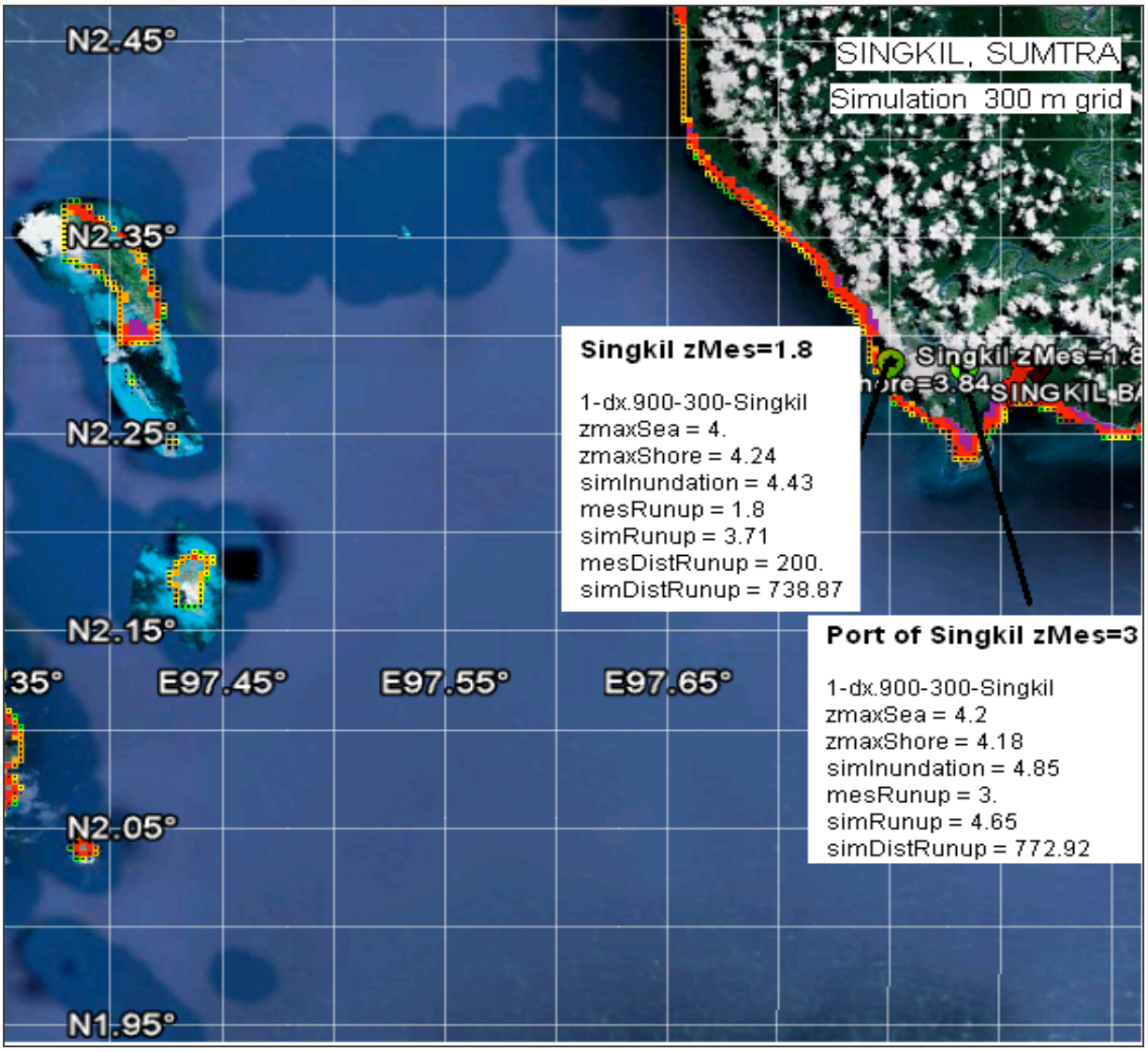

Figure 3.9. Sites in Sumatra Island where calculations could be compared with field measurements.

3.4.2 Simeulue Island: grid 2

The fishing village of Kariya Vhapi on the NW shore of Simuelue, was affected by a flow higher than 3.2 m that overtopped a high berm (USGS, 2005). At the shoreline subestimated wave heights of 1-1.5 m were simulated. The 28 March tsunami was large at Gusong Bay, Busung **(**SW Simeulue Island**)**. The team measured tsunami run-up of 4.2 m and the simulated run-up is 3.08 m, whereas at run-up is overestimated in simulation.

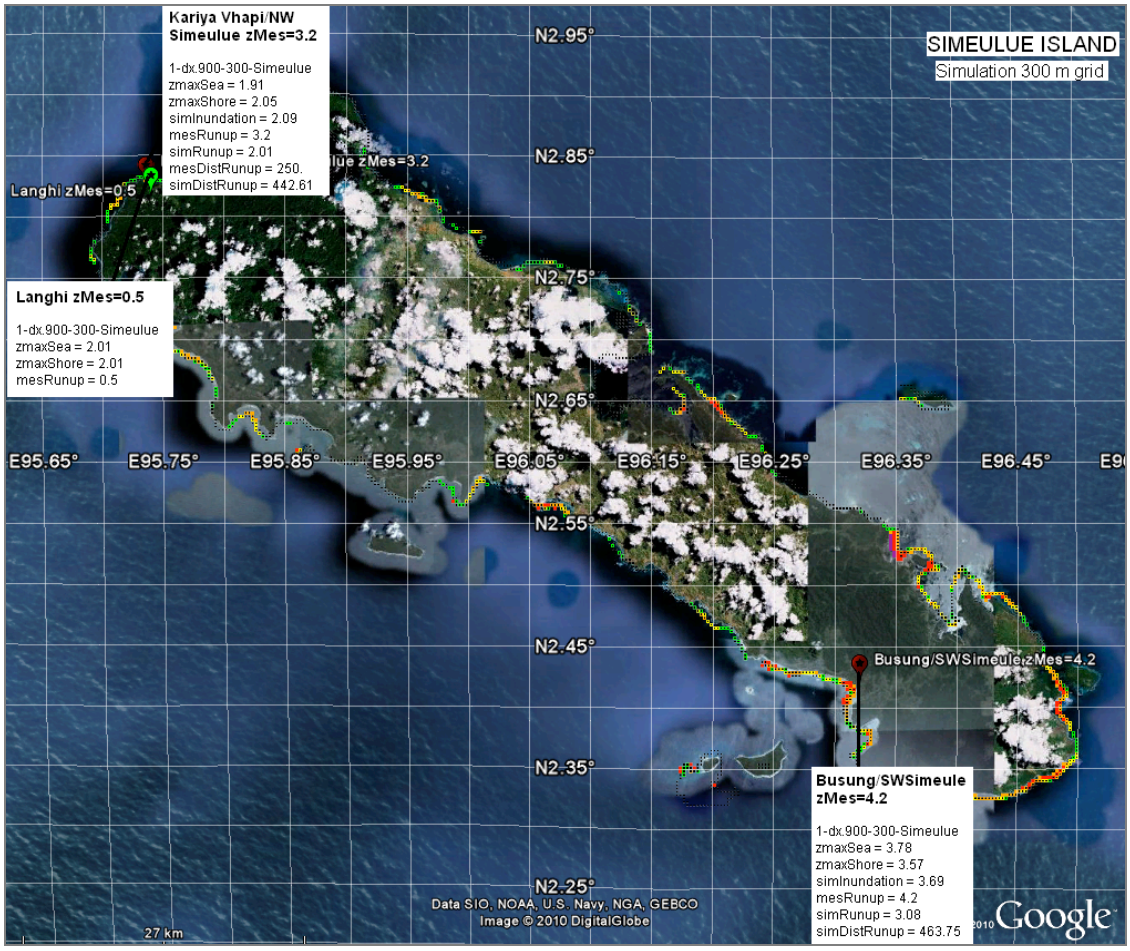

Figure 3.10 Three sites where calculations could be compared with field measurements. Ratio 0.68 (simRun-up/mesRun-up).

34.3 Nias Island: grid 3

Nias Island sites were very affected by the tsunami according to field measurements (USGS, 2005a*)*. The Nias tsunami was larger than the 26 December tsunami at Lagundri Bay in SW Nias Island. At the specific site of Lagundri Bay, SW Nias Island tsunami run-up of 3 to 4 m and inundation distances of 400 to 500 m were measured. Uplift was small here, less than 0.3 m. The tsunami arrived 5 to 15 minutes after the earthquake on 28 March. The simulated distance of 379 m is close to the 400-500 m measured for this site (Fig. 3.11; 3.12). Considering that the measured distance is in the same order of the grid size, the simulation results should be considered only qualitatively: however, the simulated maximum water height in the shoreline and the maximum run-up distance are information that can be used for early identification of the run-up areas, without to pretend to estimate in detail the amount of the inundated area.

The 28 March 2005 earthquake cause uplift in the island of Asu 1 to 2 meters, exposing coral reef. Simulated wave height offshore is 4.43 but no run-up, this could be related to high uplifted on the area.

As a final point, in order to have a reliable sea level prediction on the coast it is however necessary to use much finer nodalizations. We have used 300 m resolution grid to calculate also the inundation phase. However results of Samoa tsunami assessment using HyFlux2 where detailed bathymetry of 10 m was available showed even better performance (Franchello and Annunziato, 2012). Update Nias 2005 tsunami evaluation using new seismological and remote sensing data will be very valuable also when more fine bathymetry and topography are available.

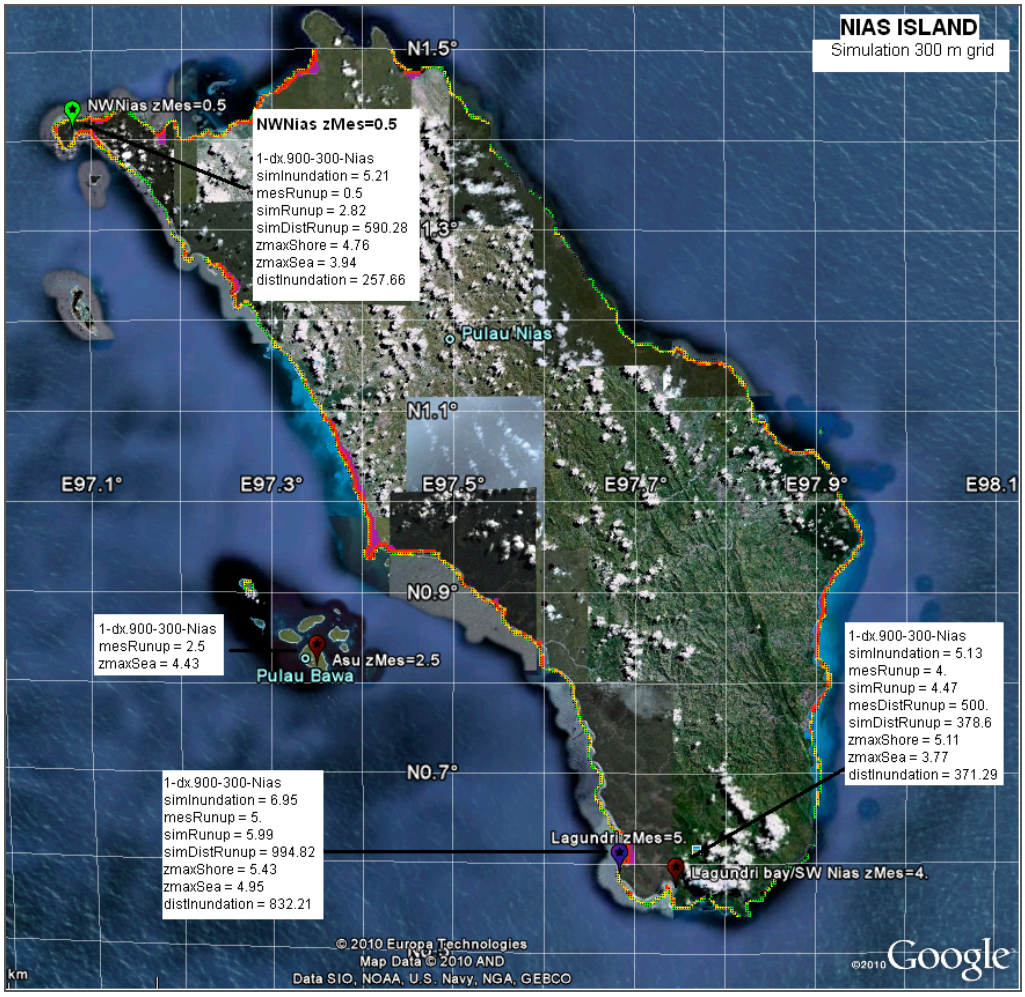

Figure 3.11. Sites where calculations could be compared with field measurements.

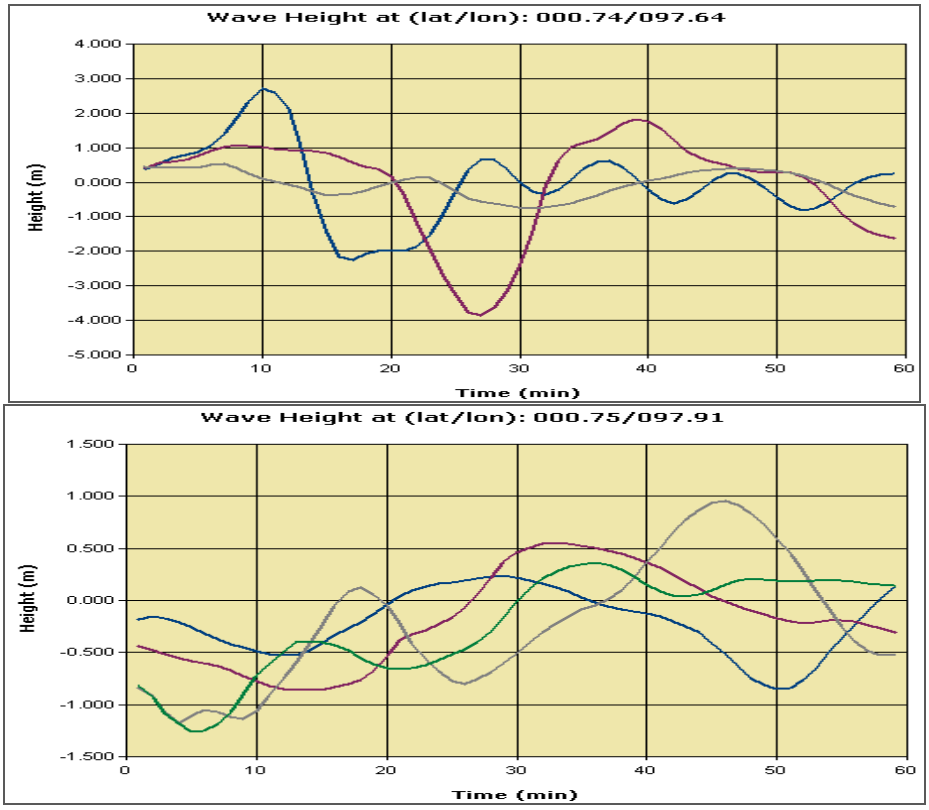

Figure 3.12. a. Sea level at south Nias: sensor S5(blue), S6 (pink) and S7 (grey). b. Sea level at S-SE Nias: sensor S8(blue), S9 (pink), S10 (grey) and S11 (green).

4. CONCLUSIONS

The tsunami analysis depends strongly on: a) the initial fault mechanism; b) the hydraulic conditions (e.g. bathymetry cell size). It is also important to point out that the information available immediately after the events are only epicenter, magnitude and depth. All these quantities may change significantly due to progressive improvement of the seismological parameters provided by the seismological centers. In addition grid resolution is very important, for example medium resolution simulations of 300 m give different results when comparing with the high resolution (5 minutes, 1 minute) as it is expected. In addition the ideal for assessing wave inundation is to have bathymetry resolution at least finer than 30 m. However, wave height trends, mainly the first wave simulated with coarser resolutions do not show great differences except when we compare the three main numerical codes under study.

Propagation results have been very reliable and consistent for the assessed codes; while for the inundation limitation still exist. In order to have a reliable sea level prediction on the coast it is

however necessary to use much finer nodalizations. This was done by using a 300 m resolution grid and the HyFlux2 code was used to calculate also the inundation phase. Considering that the measured distance were in the same order of the grid size, the simulation results can be considered qualitatively, allowing an early identification of the run-up areas, without to intend to estimate in detail the amount of the inundated area. Better bathymetry resolution could have even improved the results but it was not available. In other reports it was shown that 30 m resolution could has noticeably improved the local response.

HyFlux2 code show smoother results in the sea level trends than TUNAMI-N2 and JRC-SWAN code. In simulated wave heights resulted at the shoreline the HyFlux2 code shows less oscillations in respect to the other codes, explaining why the maximum water surface level were under estimated in respect to the other codes. HyFlux2 numerical approach makes robust performance and reliability for inundation assessment

As evaluated along Banyaks and Nias Islands where high deformation was measured on the field was not represented in fault models. Nias 2005 event was an interesting case to evaluate crustal deformation and how this deformation is being reproduced by the fault models to get the initial water column displacement. Thus, cases like 2005 Sumatra, among others, have been good cases to evaluate this approach. We can conclude that still a challenge for early warning systems to get the most reliable fault mechanism minutes after the earthquake.

ACKNOWLEDGEMENT

We acknowledge Dr. Gegar S. Prasetya for advices given at the beginning of this research. We thank Dr. Gavin Hayes (USGS) for providing Finite Fault Model of Northern Sumatra (Nias) earthquake. Figure 1 has been done using GMT 4.5.8. N.Z Acknowledge EC-JRC for training program in tsunami modelling.

REFERENCES

Annunziato, A. (2005). Development and Implementation of a Tsunami Wave Propagation Model at JRC. **Proceedings of the International Symposium on Ocean Wave Measurement and Analysis**. Fifth International Symposium on Ocean Wave Measurement and Analysis. Madrid 3-7.

Annunziato, A. (2007). The Tsunami Assessment Modelling System by the Joint Research Centre. *Science of Tsunami Hazards* **26:2**, 70-92.

Briggs, R.W. (2006). Deformation and slip along the Sunda megathrust in the great 2005 Nias–Simeulue earthquake. *Science* 311, 1897-1901.

Castro, C.E., Toro, E.F. and Käser, M. (2012). ADER scheme on unstructured meshes for shallow water: simulation of tsunami waves. *Geophys. J. Int.* **189:3**, 1505-1520.

Falck, C., Ramatschi, M., Subarya, C., Bartsch, M., Merx, A., Hoeberechts, J., and Schmid, G. (2010). Near real-time GPS applications for tsunami early warning systems. *Nat. Hazards Earth Syst. Sci.* **10**, 181-189.

Franchello, G. (2008). Modelling shallow water flows by a High Resolution Riemann Solver. JRC Scientific and Technical Reports. **EUR 23307** EN 34p.

Franchello, G. (2010). Shoreline tracking and implicit source terms for a well balanced inundation model. *International Journal for Numerical Methods in Fluids* **63:10**, 1123-1146.

Franchello, G. and Annunziato, A. (2012). The Samoa tsunami of 29 September 2009- Early Warning System and Inundation Assessment. *Science of Tsunami Hazards* **31:1**, 19-612.

Geist, E. L., and Dmowska, R. (1999). Local tsunamis and distributed slip at the source. Pure and Appl. Geophys. **154**, 485-512.

Geist, E., Bilek, S.L., Arcas, D. and Titov, V.V. (2006). Differences in tsunami generation between the December 26, 2004 and March 28, 2005 Sumatra earthquakes. *Earth Planets Space* **58,** 185-193.

Geist, E., Titov, V.V., Arcas, D. Pollitz, F.P. and Bilek, S.L. (2007). Implications of the December 26, 2004 Sumatra-Andaman earthquake on tsunami forecast and assessment models for great subduction zone earthquakes. *Bull. Seis. Soc. .Amer*. **97, 1A,** S249-S270.

Goto, C., Ogawa, Y., Shuto, N. and Imamura, F. (1997). Numerical Method of Tsunami Simulation with the Leap-Frog Scheme. IUGG/IOC TIME Project Intergovernmental Oceanographic Commission of UNESCO. *Manuals and Guides* **36:26**, 126 p.

Imamura, F. (1996). Simulation of wave-packet propagation along sloping beach by TUNAMI-code: Long-wave Run-up Models edited by H.Yeh, P.Liu and C.Synolakis. World Scientific I981, 231-241 p.

Imamura, F., Yalciner, A.C. and Ozyurt, G. (2006). Tsunami Modeling manual - TUNAMI-N2 (Tohoku University's Numerical Analysis Model for Investigation of Near Field Tsunamis ver. 2) http://www.tsunami.civil.tohoku.ac.jp/hokusai3/J/projects/manual-ver-3.1.pdf. (Accessed 02/15/2010).

Ji, C., Wald, D.J. and Helmberger, D.V. (2002). Source description of the 1999 Hector Mine, California earthquake; Part I: Wavelet domain inversion theory and resolution analysis. *Bull. Seis. Soc. Am*er. **92:4**, 1192-1207.

Liu, P., Yeh, H., Lin, P., Chang, K.T. and Cho, Y.S. (1998). Generation and evolution of edge-wave packets, Phys. Fluids **10**: 7, 1635-1657.

Mader, C.L. (1974). Numerical Simulation of Tsunamis. *J. Phy. Ocean.* **4:** 74.

Mader, C.L. (1988). Numerical modeling of water waves. University of California Press, Berkeley, California.

Mader, C.L. (2004). Numerical Modeling of Water Waves. 2nd ed., CRC Press, Boca Raton, Fl. 274p.

McCaffrey, R. (2009). The Tectonic Framework of the Sumatran Subduction Zone. Annu. *Rev. Earth. Planet. Sci.* **37**, 345-366.

NOAA, National Oceanic and Atmospheric Administration website: http://nctr.pmel.noaa.gov/tda_documentation.html. (Accesed 11/15/2010).

Okada, Y. (1985). Surface deformation due to shear and tensile faults in a half-space. Bull. of the Seis. Soc. of Amer. **75**,1135–1154.

Prawirodirdjo, L. and Bock, Y. (2004), Instantaneous global plate motion model from 12 years of continuous GPS observations, *J. Geophys. Res.* **109**, B08405.

Sobolev, S.V, Babeyko, A., Wang, R., Galas, R., Rothacher, M., Sein, D.V., Schröter, J., Lauterjung, J. andSubarya, C. (2007). Concept for fast and reliable tsunami early warning using "GPS-Shield" arrays. *J. Geophys. Res*. **112**, B08415.

Song, Y.T. (2007). Detecting tsunami genesis and scales directly from coastal GPS stations. *Geophys Res. Lett.*, **34,** L19602.

Subarya, C., Chlieh, M., Prawirodirdjo, L., Avouac, J.P., Bock, Y., Sieh, K., Meltzner, A.J., Natawidjaja, D.H. and McCaffrey, R. (2006). Plate-boundary deformation associated with the great Sumatra–Andaman earthquake. *Nature* **440**, 46-51.

Titov, V.V., Gonzalez, F., Bernard, E.N., Eble, M.C., Mofjeld, H., Newman, J.C and Venturato, A.J. (2005). Real-Time Tsunami Forecasting: Challenges and Solutions. *Natural Hazards* **35**, 41–58.

USC - http://earth.usc.edu/~jrdonova/finite_fault_links.html

USGS, 2005a - http://walrus.wr.usgs.gov/news/reports.html. (Accesed 12/06/2012).

USGS, 2005b - http://earthquake.usgs.gov/regional/neic. (Accesed 12/06/2012).

Ward, S .N. (2002). Tsunamis. Encyclopedia of Physical Science and Technology. Ed. Meyers, R.A., Academic Press, **VOL XVII**: 175–191.

Zamora-Sauma, N., Franchello, G. and Annunziato, A. (2011). 1 April 2007 Solomon Island tsunami: case study to validate JRC tsunami codes. Joint Research Centre – Institute for the Protection and Security of the Citizen. **EUR 24783** EN, 63p.